Chemistry and Materials Research
ISSN 2224- 3224 (Print) ISSN 2225- 0956 (Online)
Vol.6 No.10, 2014
www.iiste.org

Synthesis, Characterization and Photocatalytic Activity of $MnO_2/Al_2O_3/Fe_2O_3$ Nanocomposite For Phenol Degradation

Tesfa Oluma Fufa, Abi Tadesse Mengesha Om Prakash Yadav
Department of Chemistry, College of Natural and Computational Sciences, Haramaya University, Haramaya, Ethiopia
atesfaolumaf@gmail.com, babi92003@yahoo.com, cyadavop02@yahoo.com

Abstract
Photocatalysis has become a fast wastewater treatment technology. Herein; ternary mixed oxide catalyst, phenol pollutant and visible light were used. The new $MnO_2/Al_2O_3/Fe_2O_3$ nanocomposite was synthesized by sol-gel method using $Fe(NO_3)_3.9H_2O$, $Al(NO_3)_3.9H_2O$, MnO_2, 1-C_4H_9OH and 68 % HNO_3 precursors in aqueous solution and characterized by XRD, UV-VIS, FAAS and FTIR instruments. The crystal size and the bang gap energy of $MnO_2/Al_2O_3/Fe_2O_3$ nanocomposite were found to be 20 nm and 2.25 eV, respectively. The photocatalytic activity of $MnO_2/Al_2O_3/Fe_2O_3$ nanocomposite was tested under varies operational parameters. The optimum operational parameters were found to be 10 pH, 50 $mg.L^{-1}$ C_6H_5OH, 20 $mg.L^{-1}MnO_2/Al_2O_3/Fe_2O_3$ nanocomposite, visible light presence and 3 hr irradiation time. At optimum operational parameters phenol degradation efficiency was found to be 93.1 %. The kinetic studies indicated that the pseudo first order rate constant was $01.62x10^{-2}$ $min^{-1}$for the phe-vis-cat tests. Finally, the phenol degradation mechanisms were discussed.
Keywords: Photocatalysis, $MnO_2/Al_2O_3/Fe_2O_3$ nanocomposite, phenol pollutant, visible light and operational parameters.

1. Introduction

Phenol (C_6H_5OH) is one of aromatic organic compounds that can exist naturally or synthetically (**Azni, 2002, Khazi *et al.*, 2010 and Guido *et al.*, 2008**). Industrially, it is manufactured to synthesize items such as phenolic resins, plastics, explosives, fertilizers, paints, rubbers, textiles, adhesives, drugs, papers, soaps and wood preservatives. Phenol discharges into environment during its production or application is a major source of water contamination due to its toxicity and non-biodegradability nature (**Liotta *et al.*, 2009, Mohammad *et al.* 2012**). Overexposure to phenol cause severe injuries to human internal organs including liver, kidneys, lungs and vascular system (**Shawabkeh *et al.* 2010**). The maximum allowable limit for phenol concentration in water as set by Environmental Protection Agency is 4 $mg.L^{-1}$ (**Reyad et al., 2010**). As phenol concentration gets much higher than this value, it becomes an urgent need for preventing from water resources. Therefore, various technologies including physical methods (**Sun *et al.*, 2011**), biological methods (**Basha *et al.*, 2010; Guido *et al.*, 2008; Khazi *et al.*, 2010 & Wang *et al.*, 2011**) and chemical methods (**Yan *et al.*, 2007**) have been reported to minimize the concentration of phenol in water. The physical methods (primary treatments) and the biological methods (secondary treatments) are not advantageous, since they simply transfer pollutants from one phase to another. After these treatments, there are non-biodegradable products for which the chemical methods (tertiary treatments) are needed; particularly the advanced oxidative process (AOP) that generates the strongly oxidizing hydroxyl radicals ($^{\cdot}OH$) appears cost effective for phenol pollution prevention (**Yan *et al.*, 2007**) from water.

Over past years, photochemistry of semiconductor oxides (TiO_2, ZnO, WO_3, Bi_2WO_6 and α-Fe_2O_3) has been interested in water decontamination (**Salaices *et al.*, 2004**). Semiconductor absorbs a photon of suitable energy that promotes electrons (e^-) from its valence band (VB) to its conduction band (CB); leaving behind a positive charge vacancy (h^+). To carry out a photochemical change, charge transfer reaction must compete efficiently with the recombination process which takes place within nanosecond scale. Due to this rigorous reaction, pre-adsorption of charge trapping species (e^- acceptors like O_2 and e^- donors like H_2O) are believed to lead efficient chemical reactions. Due to its high extent range and cost effective nature; visible-light driven photocatalysis for organic degradation has found widespread applications in various industries. Solar spectrum consists 7 %, 46 % and 47 % of UV light, Vis light and IR radiation, respectively (**Bak *et al.*, 2002**). Thus, visible light active catalysts have been the major focus.

Among AOPs, heterogeneous photocatalysis confirmed good efficiency for degrading many organic contaminants into CO_2, H_2O and some biodegradable mineral acids (**Liou *et al.*, 2005**). Generally, to promote adsorption of substrates on photocatalyst surface and facilitate generation of hydroxyl radicals, it must be improved by rapid charge separation, surface acidity/alkalinity and OH group population (**Xianliang *et al.*, 2012**). Nanosized α-Fe_2O_3 semiconducter based materials have been found to be good environmental catalysis. To synthesize such material needs knowledge to control its crystal size in the photocatalyst (**Kumar *et al.*, 2012**).

This is, due to the particles agglomeration in solution which causes the reduction of photocatalytic efficiency. One way to overcome this drawback is to apply solution-based chemical synthetic methodologies such as sol-gel (**Ting *et al*, 2010**), in-situ oxidative method (**Sozeri *et al.*, 2012; Ma *et al.*, 2010; & Thomas *et al*., 2009**) and chemical oxidative polymerization method (**Shukla *et al.*, 2010**) that can easily disperse the oxide in organic solvent and homogenously load on the supported material. Nanoparticle refers to size of a particle with at least one dimension from 1 nm to 100 nm (**Lovestam *et al*., 2010**). Coupling different semiconductor metal oxides together extend sample's light response to visible region and enhance photo-generated e^{-}-h^{+} separation efficiency. Recently, some studies tried to improve the photo catalytic activity of α- α-Fe_2O_3, whose band-gap energy is 2.3 eV, by coupling with different metal oxides such as Fe-Mn/SiO_2 (**Mostafa *et al*, 2012**), Al_2O_3-Fe_2O_3 (**Liu *et al.*, 2012, Yan *et al*., 2007 and Xianliang *et al*, 2012**) and Pani-MnO_2 (**Ali *et al*., 2007**). Although these mixed oxides have shown better photocatalytic activity, it is still not satisfactory for degradation of organics. **Shannon *et al.* (1976)** reported that the ionic radii of Fe^{+3}, Al^{+3} and Mn^{+4} for coordination number 6 are 59 pm, 54 pm and 53 pm, respectively. Here, for the first time, we reported the synthesis (by sol-gel method), characterization (by XRD, UV-VIS, FAAS and FTIR) and photocatalytic activity (by different operational parameters) of $MnO_2/Al_2O_3/Fe_2O_3$ nanocomposite on aqueous phenol. Additionally, we have discussed phenol degradation mechanisms over the $MnO_2/Al_2O_3/Fe_2O_3$ nanocomposite.

2. Experimental

2.1. Sol-Gel Synthesis of $MnO_2/AlO_3/Fe_2O_3$ Nanocomposite

$MnO_2/Al_2O/Fe_2O_3$ nanocomposite was synthesized by acid catalyzed sol-gel method (**Deheri *et al*., 2010**, **John *et al.*, 2006, Kirszensztejn *et al*, 2003, Kyeong *et al*, 2004**), as followings. $Fe(NO_3)_3.9H_2O$ (28.28 g), $Al(NO_3)_3.9H_2O$ (7.50 g), MnO_2 (0.87 g) and 1-C_4H_9OH (16 g, 20 mL or 0.22 mol) were added into a separate 200 mL beaker containing 28 mL, 8 mL, 4 mL and 0 mL distilled water, respectively, and stirred continuously by magnetic stirrer until dissolved. Each solution was mixed together into another 200 mL beaker containing 3 mL of conc.HNO_3 and stirred by magnetic stirrer for 10 min to dissolve. Then the solution was left undisturbed for 5 days at room temperature to make gel. After gelation, the gel was heated at 100 ^{o}C for 36 h in electric oven to evaporate the excess-solvents and to dry. Then the dry gel was divided into three portions and transferred to crucible and calcinated at 400 ^{o}C, 600 ^{o}C and 800 ^{o}C for 3 h in electric furnace, respectively to burn out unnecessary organics. Then, the samples cooled down gradually to room temperature to avoid thermal shocks, milled with mortar and pestle to make fine powder and to get a red purple powder. The resulting samples were designated based on their calcination temperatures as $S_{a\text{-}400}$, $S_{a\text{-}600}$ and $S_{a\text{-}800}$. These were then kept in separate polyethylene container and stayed in desiccators until further investigations. In the same manner, other $MnO_2/Al_2O/Fe_2O_3$ nanocomposite powder series were prepared by same procedures, different precursor ratios and calcination temperatures for 3 hr as shown in the following table.

Table-2.1: Designations, Compositions and Calcination Temperatures of $MnO_2/Al_2O/Fe_2O_3$ nanocomposite Samples

Code	Metal Precursor Composition									Cal.T (^{o}C)
	gram			mole			molar percentage			
	Fe	Al	Mn	Fe	Al	Mn	Fe	Al	Mn	
$S_{a\text{-}400}$	28.28	7.500	0.870	0.070	0.020	0.010	70	20	10	400
$S_{a\text{-}600}$	28.28	7.500	0.870	0.070	0.020	0.010	70	20	10	600
$S_{a\text{-}800}$	28.28	7.500	0.870	0.070	0.020	0.010	70	20	10	800
$S_{b\text{-}400}$	32.32	5.625	0.435	0.080	0.015	0.005	80	15	5	400
$S_{b\text{-}600}$	32.32	5.625	0.435	0.080	0.015	0.005	80	15	5	600
$S_{b\text{-}800}$	32.32	5.625	0.435	0.080	0.015	0.005	80	15	5	800
$S_{c\text{-}400}$	34.34	3.750	0.435	0.085	0.010	0.005	85	10	5	400
$S_{b\text{-}600}$	34.34	3.750	0.435	0.085	0.010	0.005	85	10	5	600
$S_{b\text{-}800}$	34.34	3.750	0.435	0.085	0.010	0.005	85	10	5	800

2.2. XRD Characterization of $MnO_2/Al_2O_3/Fe_2O_3$ Nanocomposite

Crystal size and structure of $MnO_2/Al_2O_3/Fe_2O_3$ samples were checked by X-Ray Diffractometer (XRD, BRUKER D8 Advanced XRPD) equipped with a Cu target for generating a Cu $_{K\alpha}$ radiation with $\lambda = 0.15406$ nm. The accelerating voltage and the applied current were 40 KV and 30 mA, respectively. The instrument was operated under 1 sec step scan and 0.020° (2θ) for 4° to 64°. Using the XRD Data and Dubye Scherrere's Equation, the smallest crystallite size of $MnO_2/Al_2O_3/Fe_2O_3$ series was found to be 20 nm which is for the 5%Mn/10%Al/85%Fe at 400 ^{o}C. Thus, it was selected for further studies (i.e., for UV-VIS Study, FTIR Study and Catalytic Activity).

2.3. UV-VIS Characterization of $MnO_2/Al_2O_3/Fe_2O_3$ Nanocomposite

To determine the absorption edge of synthesized and selected samples, UV-VIS Spectrophotometer (SANYO, SP65) was used. The $MnO_2/Al_2O_3/Fe_2O_3$ sample was dissolved in 1M HCl aqueous solution, absorption of each was measured at 200-800 nm wavelengths range and the data were recorded.

2.4. FTIR Characterization of $MnO_2/Al_2O_3/Fe_2O_3$ Nanocomposite

To determine bond structure of synthesized and selected $MnO_2/Al_2O_3/Fe_2O_3$ samples, FTIR Spectrometer (FTIR-65, Perkin-Elmer) was used. First, at room temperature, the instrument was adjusted with a resolution of 4 cm^{-1}, accumulating 100 scans, between 400 cm^{-1} and 4000 cm^{-1} wave numbers. Second, 0.001 g of each sample was mixed with 0.1 g of KBr and ground to a fine powder, respectively. Then, a transparent disc was formed using a nitrogen pressure in moisture free atmosphere for 1 h and absorption was recorded.

2.5. FAAS Characterization of $MnO_2/Al_2O_3/Fe_2O_3$ Nanocomposite

Percentages of each metal in $MnO_2/Al_2O_3/Fe_2O_3$ were determined by Flame Atomic Absorption Spectrophotometer (FAAS, Model 210/211, Karisruh, West Germany). First, 1L 1000 $mg.L^{-1}$ $Fe(NO_3)_3.9H_2O$, 1L 1000 $mg.L^{-1}$ $Al(NO_3)_3.9H_2O$ and 1L 1000 $mg.L^{-1}$ MnO_2 was prepared in DI H_2O, respectively. From each solution, by Dilution Law, five standard solutions were prepared and absorbance was recorded to plot calibration curves, (Fig-3.1-3). Second, $MnO_2/Al_2O_3/Fe_2O_3$ (0.01 g) was digested with 68% HNO_3 (8 mL), 38% HCl (5 mL) and 30% H_2O_2 (3 mL) in acid digestion tube till clear solution appeared (30 min). Then the solution was filtered, diluted to 100 mL, designated as N_1. In similar manner, triplicate $MnO_2/Al_2O_3/Fe_2O_3$ samples were prepared for each metal and absorbance were recorded, (Table-2.2). Finally, percentage of each metal was calculated using linear equations obtained from the respective calibration curves, (Fig-3.1-3).

Table-2.2: Samples Prepared for FAAS Analysis of Metals in $MnO_2/Al_2O_3/Fe_2O_3$ Nanocomposite

	Fe^{+3}		Al^{+3}		Mn^{+4}	
	ppm	**Abs**	**ppm**	**Abs**	**ppm**	**Abs**
Digested Blank Sample S_0	0	0	0	0	0	0
Precursor Standard S_1	10	0.17	1	0.023	2	0.098
Precursor Standard S_2	20	0.303	2	0.041	4	0.155
Pre_3cursor Standard S_3	40	0.561	4	0.076	6	0.369
Precursor Standard S_4	80	1.1585	8	0.157	8	0.653
Precursor Standard S_5	120	1.5717	12	0.213	12	0.981
Digested Sample N_1	x_1	1.1297	x_4	0.208	x_7	0.457
Digested Sample N_2	x_2	1.1225	x_5	0.204	x_8	0.453
Digested Sample N_3	x_3	1.1398	x_6	0.207	x_9	0.456

2.6. Photocatalytic Activity of $MnO_2/Al_2O_3/Fe_2O_3$ Nanocomposite

To investigate, $MnO_2/Al_2O_3/Fe_2O_3$ catalytic activities towards visible light induced phenol degradation, the overall procedures were as followings. Firstly, at room temperature of laboratory scale, photocatalytic reactor was adjusted with 200 mL samples beaker and a 300 W Xenon Lamp (PLS-SXE300, Trusttech Co. Ltd., Beijing, intensity: ~700 mW cm^{-2} at λ=420 nm, 420 nm $\leq \lambda \leq$ 760 nm) that was hanged over the sample beaker at 20 cm distances. Secondly, the UV-VIS Spectrometer was adjusted with computer and wavelength was adjusted at 270 nm which is λ_{max} of aqueous phenol. Remember, this λ_{max} was matched with the λ_{max} reported by **Li *et al.*, (2008)** and **Wenzong *et al.*, (2010)**. Thirdly, 100 mL of 50 ppm aqueous phenol at pH 10 was prepared and its absorbance was measured before light irradiation and the data are recorded. Then, the prepared solution was mixed with 20 mg of $MnO_2/Al_2O_3/Fe_2O_3$ powder and the suspension was stirred using magnetic stirrer in dark condition for 30 min to establish adsorption-desorption equilibrium between the $MnO_2/Al_2O_3/Fe_2O_3$ catalyst and the phenol pollutant. Then, the solution was irradiated with the visible light while oxygen flowing in the system through a reactor hole. As the reaction proceeded, 5 mL suspension was taken at each 20 min time intervals and centrifuged at 6000 rpm for 10 min, filtered through 0.22 mm pore size filter paper to remove the catalyst particles, the phenol filtrate absorptions were measured, and the data were recorded, until 180 min. The absorption data were converted to concentration though Beer-Lambert Law calibration curve. Remember that the absorption and concentration of a sample has a direct proportionality. The term phenol degradation efficiency (R), is used to quantify the degree of water purified from phenol, is defined as the percentage of phenol removed from the solution under the given experimental conditions. Thus, the data obtained from the experiments were used to calculate the phenol degradation efficiency (R) as following.

R = {[(A_0-A_t) ÷ A_0] x 100} …….. (Equation-1), where, **R** is degradation percentage of phenol, $\mathbf{A_0}$ is the initial absorbance of phenol and $\mathbf{A_t}$ is at-time-t absorbance of phenol.

3. Results and Discussion

3.1. FAAS Study of $MnO_2/Al_2O_3/Fe_2O_3$ Nanocomposite

Metal percentages were calculated using linear Equations of the calibration curves, plotted below.

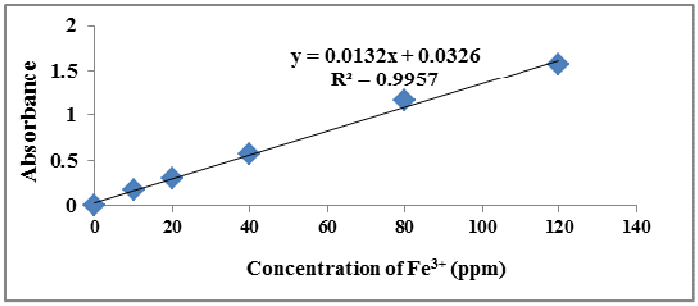

Figure-3.1: Calibration curve for Fe ion (FAAS Reading)

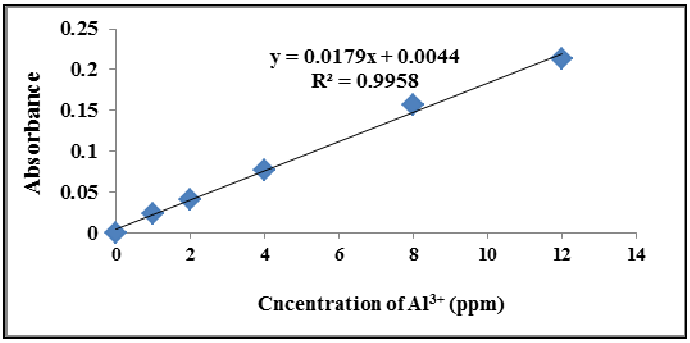

Figure-3.2: Calibration curve for Al ion (FAAS Reading)

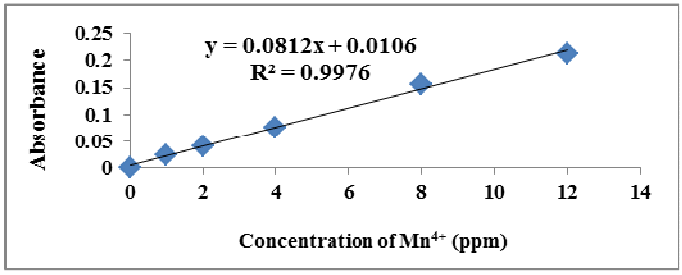

Figure-3.3: Calibration curve for Mn ion (FAAS Reading)

So, percentage of each metal in $MnO_2/Al_2O_3/Fe_2O_3$ was almost similar with the measured during the synthesis.

Table 3.1: Calculated Percentages of Fe, Al and Mn oxides from synthesized powders.

Sample Formula	%Fe[a]	%Fe[b]	%Mn[a]	%Mn[b]	%Al[a]	%Al[b]
$MnO_2/Al_2O_3/Fe_2O_3$	85.0	83.2	5.0	5.5	10.0	11.3

***a** is initial percentages of as-synthesized sample & **b** is calculated percentages of synthesized sample from FAAS*

3.2. XRD Pattern Study of $MnO_2/Al_2O_3/Fe_2O_3$ Nanocomposite

XRD pattern of $MnO_2/Al_2O_3/Fe_2O_3$ reveals rhombohedral structure and hematite phase (α-Fe_2O_3). The peaks at 2θ = 24.400 °, 33.383, 36.000, 49.500, 54.200 & 62.500 were due to hematite (**Kumar *et al.*, 2012**). The data does not show any Al_2O_3 and MnO_2 presence because they may entered into Fe_2O_3 lattice as their small ionic radius size. **Shannon *et al.*, (1976)** reported that the ionic radii of Fe^{+3}, Al^{+3} & Mn^{+4} for coordination number 6 are 59 pm, 54 pm & 53 pm, respectively. In other word, the large amount of Fe_2O_3 loaded into the system during synthesis may cause insignificance of Al_2O_3 and MnO_2 on the XRD data.

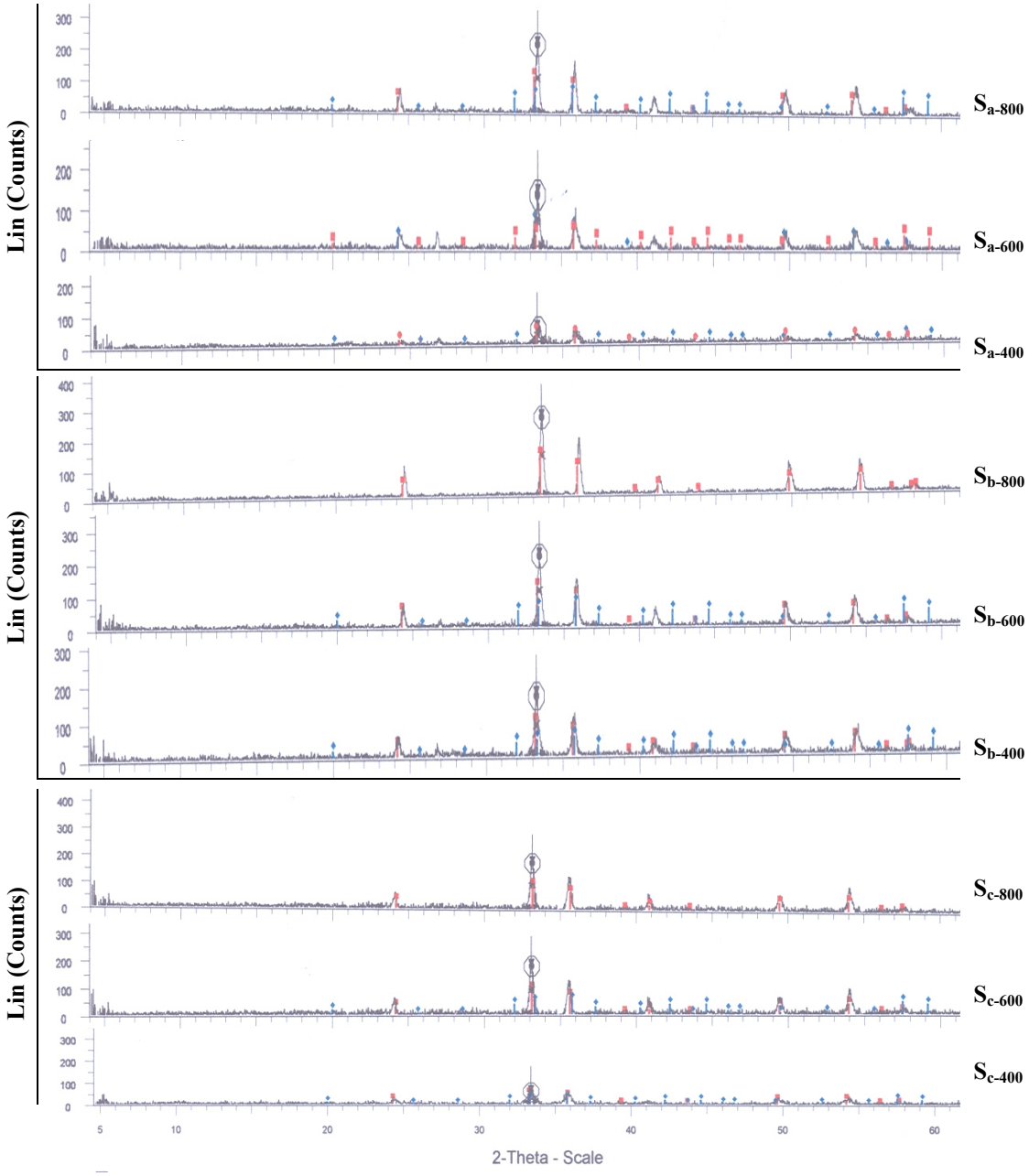

Figure 3.4**:** XRD Pattern of $MnO_2/Al_2O_3/Fe_2O_3$ with different compositions and different calcinations temperatures

The particle size of synthesized samples (D in nm), taking the most intense peak are calculated by Debye-Scherrer Equation (**Li *et al.*, 2008 and Zheng and Wu, 2009)** as follows:

$$D = k\lambda \div \beta\cos\theta \quad \text{(Equation-2)},$$

where, k is shape factor (0.94), β is full width at half maximum (FWHM) in radians, λ is X-ray wavelength (1.5406 Å = 0.15406 nm) for Cu target K_α radiation and θ is Bragg's diffraction angle in radians. Using Equation-2, crystallite sizes of samples were calculated as in Table-3.

Table 3.2: Crystal size of $MnO_2/Al_2O_3/Fe_2O_3$ Nanocomposite

№	Sample Code	Metal Perecusor (molar percentage)	Cal.T. (°C)	WL, λ (Å)	FWHM, β (°)	Angle, θ (°)	Size, D (nm)
1.	$S_{a\text{-}400}$	70Fe:20Al:10Mn	400	1.5406	0.206	16.6630	40
2.	$S_{a\text{-}600}$	70Fe:20Al:10Mn	600	1.5406	0.312	16.7200	27
3.	$S_{a\text{-}800}$	70Fe:20Al:10Mn	800	1.5406	0.254	16.7330	33
4.	$S_{b\text{-}400}$	80Fe:15Al:05Mn	400	1.5406	0.279	16.6320	30
5.	$S_{b\text{-}600}$	80Fe:15Al:05Mn	600	1.5406	0.259	16.6880	32
6.	$S_{b\text{-}800}$	80Fe:15Al:05Mn	800	1.5406	0.237	16.7865	35
7.	$S_{c\text{-}400}$	85Fe:10Al:05Mn	400	1.5406	0.417	16.6915	20
8.	$S_{c\text{-}600}$	85Fe:10Al:05Mn	600	1.5406	0.292	16.5430	28
9.	$S_{c\text{-}800}$	85Fe:10Al:05Mn	800	1.5406	0.293	16.5430	28

As it is evident from the above table, all synthesized powders are ranged in nanosized and the $S_{c\text{-}400}$ has got the smallest crystalline size, and hence with the greatest surface area. This sample was further subjected to FTIR, UV-VIS and FAAS characterization.

3.5. FTIR Spectra Study of $MnO_2/Al_2O_3/Fe_2O_3$ Nanocomposite

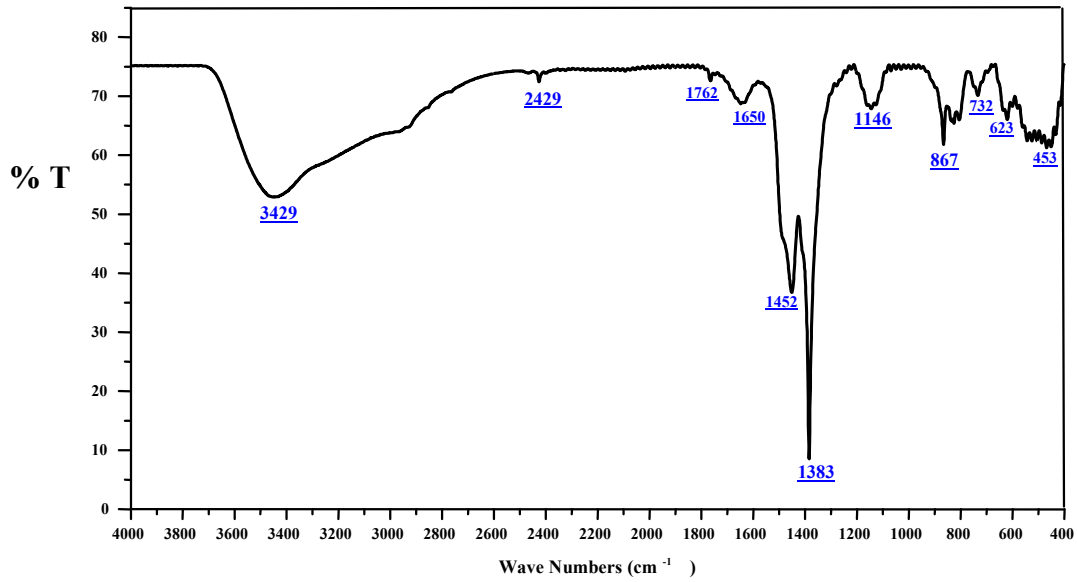

Figure 3.7: FT-IR Spectra of the as-synthesized $MnO_2/Al_2O_3/Fe_2O_3$ Nanocomposite

FTIR spectra of the synthesized $MnO_2/Al_2O_3/Fe_2O_3$ though sol gel method and calcinated at 400 ^{0}C is presented (Fig-3.7).The intense bands at 3429 cm^{-1}, 1383 cm^{-1} & 732 cm^{-1} may be due to the stretching, in-plane bending and out-plane bending of hydroxide group (–OH) from adsorbed water in the sample. The broad peak at 867 cm^{-1} is for the bending vibration mode for bridging OH group. The bands found around the wave numbers 2429 cm^{-1}, 1762 cm^{-1} & 1650 cm^{-1} are due to the OH bending vibration mode of water molecules. The sharp peak at 1146 cm^{-1} may be due to C-O stretching vibration of primary alcohol which was used to support the sol gel synthesis; while bands observed at 1452 cm^{-1} may be attributed to the –C–H, $-CH_2$ & $-CH_3$ functional groups bending vibrations.

The peaks obtained at 623 cm^{-1}, 528 cm^{-1} & 453 cm^{-1} indicates Fe-O bond presence in the sample and some interactions among iron (III), Al (III) & Mn(IV) though oxygen or hydroxide bridge. Thus, $MnO_2/Al_2O_3/Fe_2O_3$ has hydrous tri-metal composite. Additionally, results confirm adsorbed water presence on the sample surface at low temperature & short aging time (**Kumar *et al.*, 2012**).

3.6. UV-VIS Spectra Study of $MnO_2/Al_2O_3/Fe_2O_3$ Nanocomposite

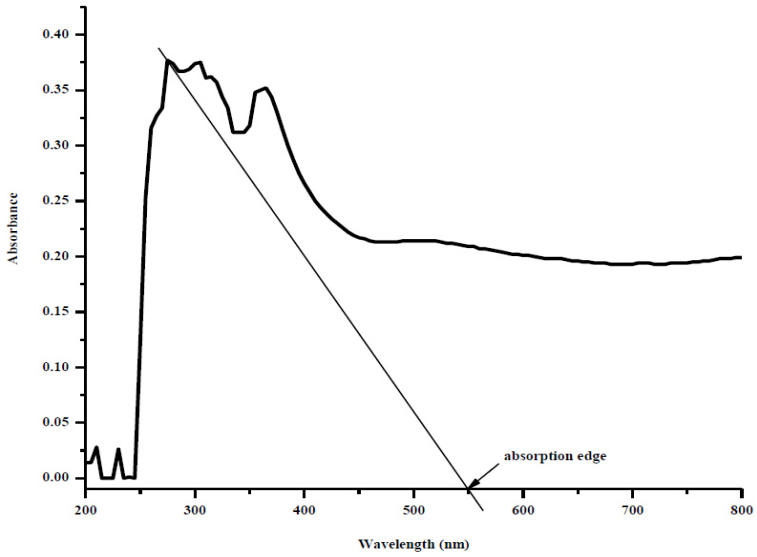

Figure 3.11**:** UV-VIS Absorption Spectra of $MnO_2/Al_2O_3/Fe_2O_3$ in 1 M HCl solvent.

UV-Vis spectra of $MnO_2/Al_2O_3/Fe_2O_3$ were subjected to strong absorption in the visible light region (Figure-3.11). Based on this, band gap energy of the material can be calculated using the following Eqn:

$$E_g = 1240/\lambda_g \quad \text{.....(Equation-3),}$$

where, E_g is band gap energy (eV) and λ_g is absorption edge wavelength (nm).

Accordingly, λ_g of $MnO_2/Al_2O_3/Fe_2O_3$ was determined to be 550 nm which corresponds to E_g = 2.25 eV. This is almost similar with the reported data of **Khasim *et al*., (2011)** for Fe_2O_3 (Eg = 3.19 eV).

3.7. Photocatalytic Degradation Study of $MnO_2/Al_2O_3/Fe_2O_3$

The photocatalytic activities of $MnO_2/Al_2O_3/Fe_2O_3$ catalyst were tested, under various operational parameters.

3.7.1. Effect of pH Values

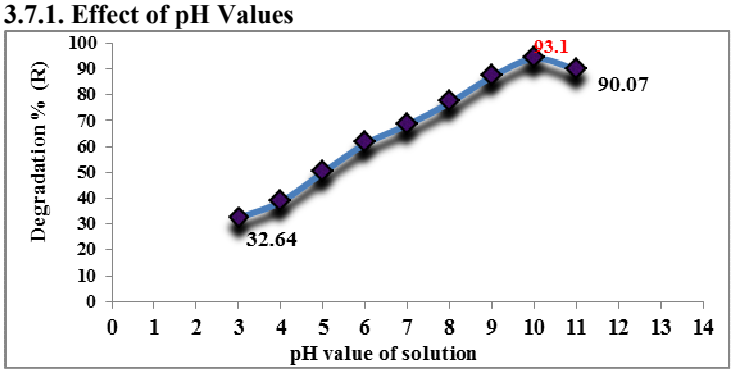

Figure 3.14: Effect of pH on phenol photodegradation in 180 min [C_{cat}=10 mg.L^{-1} and C_{phe} = 50 mg.L^{-1}].

To study pH effect on catalytic efficiency of $MnO_2/Al_2O_3/Fe_2O_3$, experiments were conducted at pH ranging from 3 to 11. The results (Figure 3.14) shows that the phenol degradation efficiency was increased from 32.64 % to 93.1 % from pH 3 to pH 10, respectively and decreased from 94.05 % to 90.07 % from pH 10 to 11, respectively in 180 min. These may be due to the more formation of hydroxyl radicals resulted from the excess hydroxyl anions used as alkaline medium. Beyond pH 10 (for higher pH) the catalyst surface becomes negatively charged and causes electrostatic repulsion between the catalyst and negatively charged phenols, as a result degradation efficiency decreased. Since the photo degradation was most effective at pH 10, the next experiments were continued with pH 10.

3.7.2. Effect of Phenol Concentrations

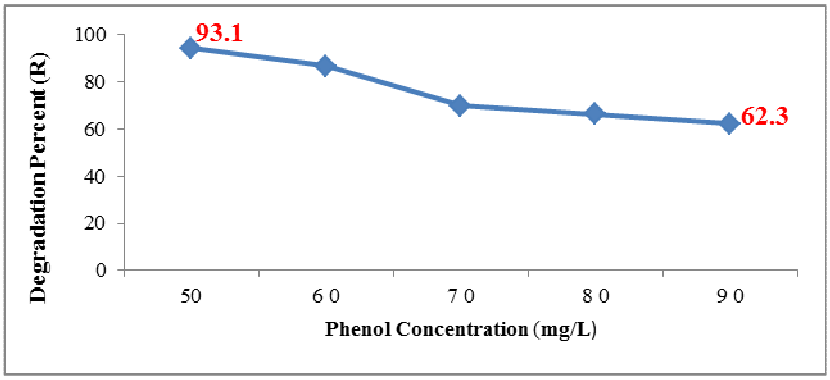

Figure 3.15: Effect of phenol concentration on phenol degradation in 180 min (C_{Cat}=10 mg/L & pH=10).

Figure 3.15 presents that phenol degradation efficiency was inversely affected by the phenol concentrations (50, 60, 70, 80 and 90 mg.L^{-1}) with 10 mg.L^{-1} cat at pH 10 within 180 min. This may be due to the equilibrium adsorption of phenol on the catalyst surface that results decrease in active sites and lower formation of $OH^{\cdot}$ radicals. According to Beer Lambert Law (A= abC), as the concentration increases, the photons path length entering the solution decreases. This results lower photon adsorption on the catalyst and decreases the photocatalytic degradation efficiency. Hence, the next experiments were continued with 50 mg.L^{-1} phenol.

3. 7.3. Effect of Catalyst Concentrations

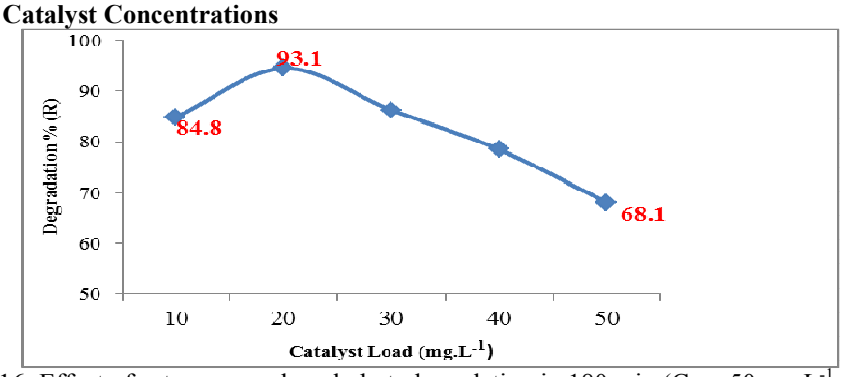

Figure 3.16: Effect of cat conc on phenol photodegradation in 180 min (C_{phe}=50 mg.L^{-1} & pH=10).

Figure 3.16 illustrates that phenol degradation efficiency was affected by the catalyst concentrations (10, 20, 30, 40 & 50 mg.L^{-1}) with 50 mg.L^{-1} phe at pH 10 within 180 min. $MnO_2/Al_2O_3/Fe_2O_3$ showed highest degradation of 93.1 % for the 20 mg.L^{-1} in 180 min. The remaining dosages' degradation efficiency was less and at10 mg.L^{-1}, it was recorded 84.8 % in 180 min. The increase in degradation rate can be explained in terms of availability of active sites on the catalyst surface and visible light penetration into the suspension as a result of increased screening effect and scattering of light. Further increase in the catalyst beyond 20 mg.L^{-1} decreases the photodegradation efficiency that may be due to the overlapping of adsorption sites of catalyst. So, the rest experiments were continued with 20 mg.L^{-1} catalyst, since it was the most effective.

3.7.4. Effect of Visible light Irradiation

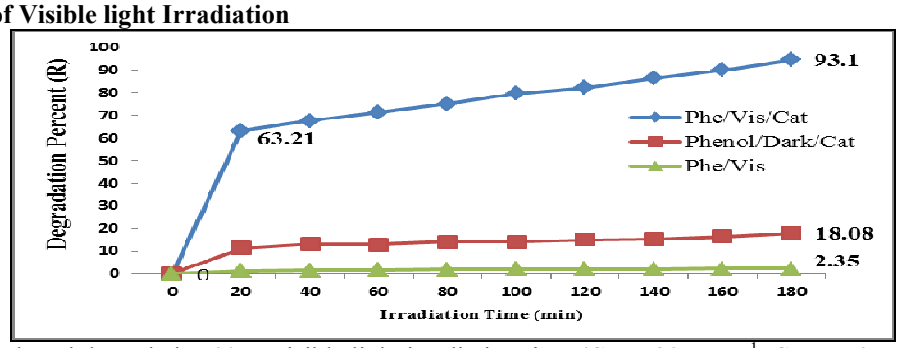

Figure 3.17: Phenol degradation % vs visible light irradiation time (C_{cat} = 20 mg.L^{-1}, C_{phe} = 50 mg.L^{-1}, pH=10, T= 25 ^{o}C).

To investigate visible light irradiation effect on catalyst-pollutant interaction, three experimentals (phenol-visible-cat tests, blank tests & dark tests) were done using C_{cat} = 20 mg.L^{-1}, C_{phe} = 50 mg.L^{-1} pH=10. Blank tests were performed under visible light without addition of catalyst and results 2.35 % R that may be due to the solutions bubbled with O_2. In addition, phenol's maximum absorption was at 270 nm wavelength and has no absorptions in visible region. Dark tests were also done in presence of catalyst and phenol solution but in absence of light. The degradation results 18.08 % R which may be due to adsorption mechanism. Generally, phenol degradation rate was found to be increase with irradiation time and visible light presence (i.e., 2.35 %, 18 % & 93.1 %) for the three experimental, respectively.

3.8. Kinetic Studies of Phenol Photocatalytic Degradation

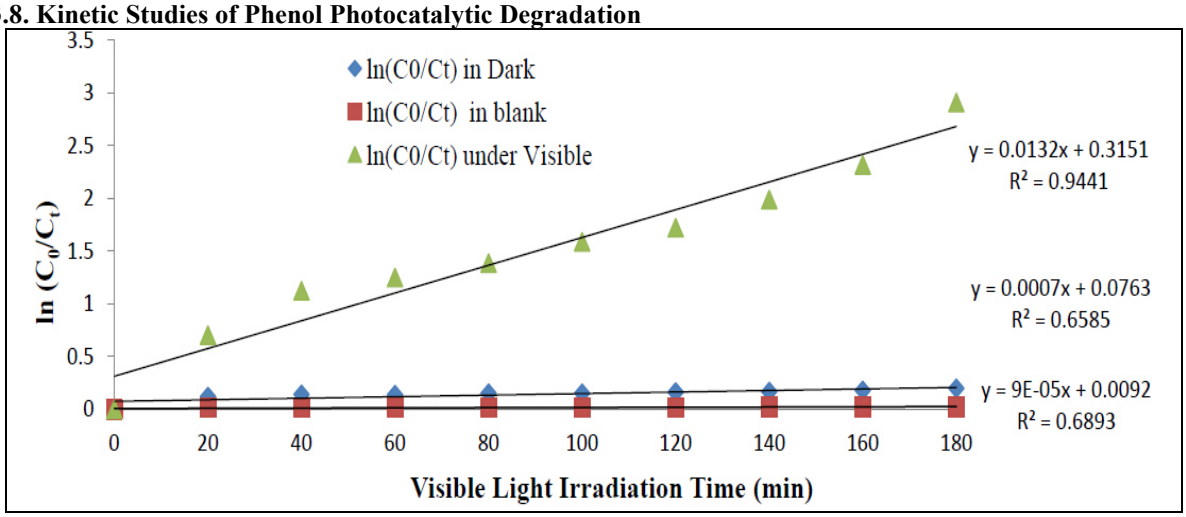

Figure 3.18: Plots of ln (C_0/C_t) vs irradiation time for photocatalytic degradation of phenol.

Since only one reactant is participated, phenol degradation follows pseudo first-order rxn equation:

$$\mathbf{kt = \ln(C_0/C_t)} \quad \text{..... (Eqn-4)}$$

where, k is reaction rate constant in min^{-1}, C_0 is initial phenol concentration & C_t is phenol concentration at reaction time t.

The linear plots of lnC_o/C_t vs visible light irradiation time were shown in Figure-3.18 and values were presented in Table-5. The calculated phenol adsorption rate constant using $MnO_2/Al_2O_3/Fe_2O_3$ was 1.62x 10^{-2} min^{-1}, 1.11 x 10^{-3} min^{-1} & 1.31 x 10^{-4} min^{-1} for phe-vis-cat tests, dark tests and blank tests, respectively. Also the correlation coefficient (R^2) of the pseudo-first order reaction found to be 0.9441, 0.6585 and 0.6893 for phe-vis-cat tests, blank tests and dark tests, respectively.

Table-3.1: ln(C_0/C_t) as function of time in Blank, in Dark and in Visible Light

Time (min)	ln(C_0/C_t) in blank	ln(C_0/C_t) in Dark	ln(C_0/C_t) under Visible
0	0.0000	0.0000	0.0000
20	0.0140	0.1220	0.7040
40	0.0164	0.1418	1.1245
60	0.0175	0.1392	1.2499
80	0.0187	0.1526	1.3866
100	0.0211	0.1526	1.5888
120	0.0211	0.1635	1.7223
140	0.0223	0.1689	1.9886
160	0.0223	0.1800	2.3166
180	0.0235	0.1996	2.9091

3.9. Mechanism of Phenol Photocatalytic Degradation

$MnO_2/Al_2O_3/Fe_2O_3$ acts as either an electron donor or an acceptor for molecules in the surrounding medium (Figure-3.1). Degradation mechanism of phenol over the $MnO_2Al_2O_3/Fe_2O_3$ surface is initiated by the absorption of a photon that equals/exceeds its band gap energy (2.25 eV), producing electron-hole (e^--h^+) pairs. h^+_{vb} is strongly oxidizing and e^-_{cb} is strongly reducing. The h^+_{vb} can either be trapped at the $MnO_2/Al_2O_3/Fe_2O_3$ surface

or react with the adsorbed species such as water, hydroxide ion, phenol compounds and oxygen. Similar mechanisms were reported by **Joshi *et al.*, (2011)**. At the external surface, the e^-_{cb} & the h^+_{vb} can take part in redox reactions with adsorbed species. Oxidation of H_2O/OH^- by the h^+_{vb} produces the OH^-, an extremely powerful oxidant. Mechanisms of photocatalytic activity of $MnO_2/Al_2O_3/Fe_2O_3$ can be predicted below.

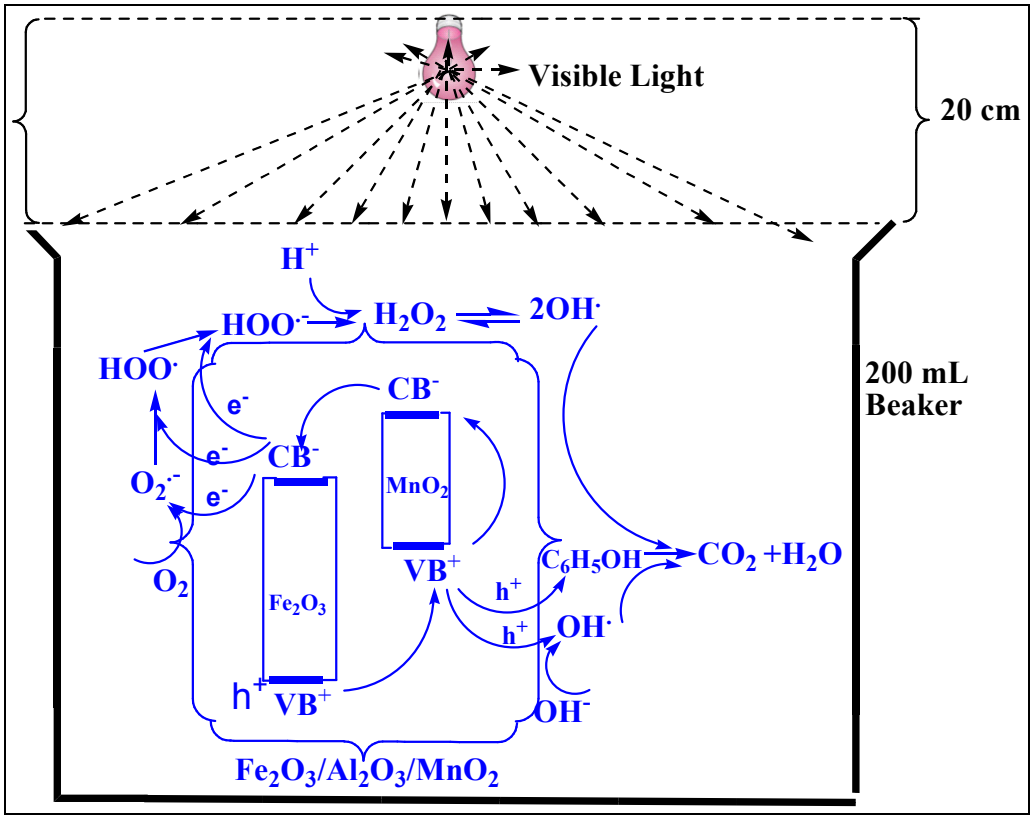

Figure 3.19: Possible Degradation Process of C_6H_5OH over $MnO_2/Al_2O_3/Fe_2O_3$ (**Tao *et al.*, 2012**)

$(MnO_2/Al_2O_3/Fe_2O_3) + hv \longrightarrow e^-_{CB} + h^+_{VB}$	(1)
$h^+_{tr} + e^-_{tr} \longrightarrow e^-_{cb}$ + heat	(2)
$4h^+ + 2H_2O \rightarrow OH^{\bullet} + 4H^+$	(3)
$h^+ + OH^- \rightarrow \underline{OH^{\cdot}}$	(4)
$e^- + O_2 \rightarrow \underline{\mathbf{O_2^{\cdot -}}}$	(5)
$O_2^{\cdot -} + H^+ \rightarrow HO_2^{\cdot}$	(5)
Phe + $OH^{\bullet}$ → Degradation Products	(6)
$C_6H_6O + 12OH^{\bullet} + 4HO\underline{O}^{\bullet} \xrightarrow{Cat/hv/O_2/H_2O} 6CO_2 + 9H_2O + 4H^-$	(7)

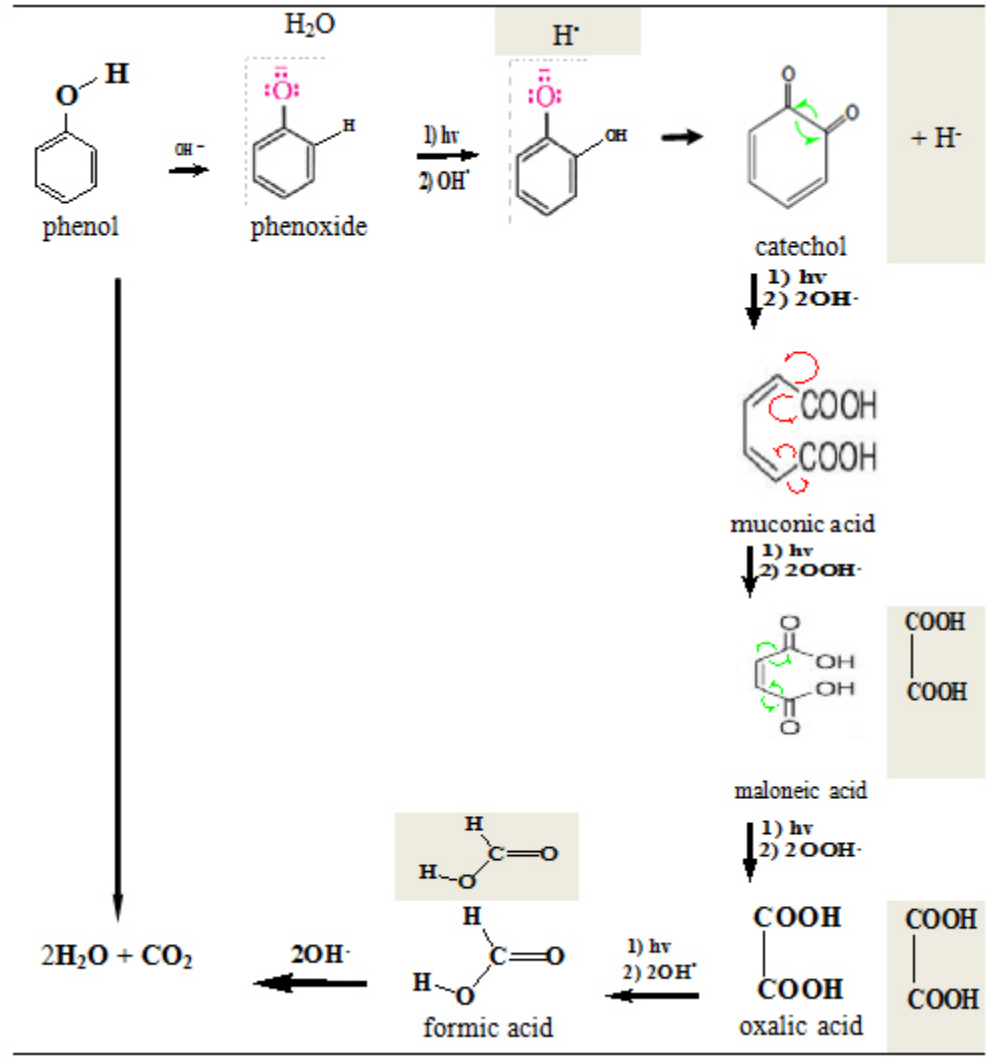

Figure 3.20: Mechanism of Phenol Oxidation by Oxidants (**Umar *et al.*, 2008, Liotta *et al.*, 2009**).

Because of its acidity (pK_a~10), phenol is easily converted into phenoxide ion in alkali media (^-OH) through free-radical mechanism in solution. $^{\bullet}OH$ radical has about 2.80 V oxidation potential and attacks the phenyl ring of the phenol, yield ring cleavage products which undergo further oxidation to various unsaturated carboxylic acids like muconic acid, maleic acid, oxalic acid, formic acid, H_2O and CO_2. Radical reaction can be classified to addition reaction, hydrogen abstraction and electron transfer.

Addition Reactions-the $^{\bullet}OH$ reacts readily with C=C double bond by addition reaction leading to a subsequent decomposition. Due to its electrophilic character, electron-rich positions at C atom are preferably attacked.

Hydrogen Abstraction Reactions-since, the bond dissociation energy of HO–H is higher than C–H bond; a H atom can be removed from phenol, thus forming a C-centered $^{\cdot}R$. The $H^{\bullet}$ radical produced during the attack of bonds by $OH^{\bullet}$ participates in the process, it is scavenged by oxygen to form peroxyl radical ($HO_2^{\bullet}$), which finally converted to $^{\bullet}OH$. Many authors proposed a chain reaction to be initiated by reaction of $^{\cdot}R$ with molecular oxygen producing a peroxyl radical that may react with organic compound and lead to CO_2 & H_2O.

Electron Transfer Reactions-the addition reaction and electron transfer are in competition although the electron transfer is thermodynamically favoured, the addition reaction is often preferred, while the direct electron transfer has been rarely observed. **Umar *et al.*, (2008) and Liotta *et al.*, (2009)** reported that $OH^{\bullet}$ radical react with phenol (C_6H_6O) to produce carbon dioxide (CO_2) and water (H_2O).

4. Conclusions

A new "MnO_2-Al_2O_3-Fe_2O_3 nanocomposite photocatalyst" was chemically synthesized by "sol-gel method"

using MnO_2-Al_2O_3-Fe_2O_3, $C_6H_5NH_2$ & $(NH_4)_2S_2O_8$, in 1M HCl solution, in laboratory level. The photocatalyst was characterized by XRD, FAAS, FTIR & UV-VIS instruments. The crystal structure, crystal phase and crystal size of the nanocomposite material was found to be a rhombohedral, hematite and 20 nm, respectively. UV-VIS absorption spectrum indicates absorption edge of $MnO_2/Al_2O_3/Fe_2O_3$ is 2.25. eV, which is an appropriate band gap for improving photocatalytic degradation of organic compounds in the visible region . Therefore, the photocatalytic activity of $MnO_2/Al_2O_3/Fe_2O_3$ was good and the results can be attributed to the synergetic effect of MnO_2, Al_2O_3 and Fe_2O_3. Several parameters have been studied to control the photocatalytic activity of $MnO_2/Al_2O_3/Fe_2O_3$ or the potodegradation rate of phenol for which optimum conditions were established for achieving maximum efficiency. It appears that the degree of phenol degradation was obviously affected by illumination time, visible light presence, catalyst concentrations, pH values and phenol concentrations. The experimental results showed that at the optimal conditions, higher degradation efficiency (93.1 %) of phenol was obtained within 3 h visible light irradiation in the presence of the catalyst. This may be due to the good absorption edge of the sample. The FTIR absorption spectra was shown that the presence of -OH and Fe-O vibration bond in the synthesized $MnO_2/Al_2O_3/Fe_2O_3$. Here, the preparation methods, characterization methods and operational parameters used for the development of the new mixed oxides nanocomposite material, truly provides a synergy not attainable separately by the individual oxide. As a result, degradation of phenol in wastewater using visible light source is an important technology in the context of our country, Ethiopia. This is due to the low operating cost and more abundance of visible light energy for pollutant removal in chemical industries and other organic processing industries. Hence, this study can be further extended with additional operational parameters such as: (annealing temperatures, aging days, degradation time, light intensities, Pani Loadings and catalyst re-uses), and additional characterization techniques such as: (SEM, TEM & XPS) are important to understand the more photocatalytic activity properties of the newly synthesized photocatalyst of $MnO_2/Al_2O_3/Fe_2O_3$ nancomposite.

5. References

Ali, H., Gemeay, G., Rehab, E.Sh., Mansour, A.I. & Zaki, A. B. (2007),"Preparation and Characterization of Pani-MnO_2 Composites and their Catalytic Activity", *Journal of Colloid and Interface Science* 308 (1), 385–394.

Azni, I., and Katayon, S., (2002), "Degradation of Phenol in Wastewater using Anolyte Produced from Electrochemical Generation of Brine Solution", *Global Nest: the International Journal* 4 (2-3), 139-1344.

Bak, T., Nowotny, J., Rekas, M., Sorrell, C.C. (2002), "Photo-Electrochemical Generation of Hydrogen from Water using Solar Energy", *Materials-related aspects, Int. J. Hydrogen Energy* 27 (4), 1022–2791.

Basha, K., Mahammedilyas, B., Rajendran, A. & Thangavelu, V. (2010), "Recent Advances in the Biodegradation of Phenol: A Review, *Asian Journal of Experimental Biological Science* 1 (3), 219-234.

Deheri, P.K., Swaminathan, V., Bhame, Sh. D., Zhongwu, L. & Ramanujan, R. V. (2010), "Sol-Gel Based Chemical Synthesis of $Nd_2Fe_{14}B$ Hard Magnetic Nanoparticles", *Chemical Mater* 30 (20), 1-9.

Guido, B., Silvia, B., Carlo, R. & Laura, A. (2008), "Technologies for the Removal of Phenol from fluid Streams: A Short Review of Recent Developments", *Journal of Hazardous Materials*, 160 (4), 265–288.

John, K.L., Vijaya, J. J., Sekaran, G., Joseph, J., Rani, J. D. & Pragasam, J. (2006), "Bulk preparation and Characterization of Mesoporous Carbon Nanotubes by Catalytic Decomposition of Cyclohexane on sol–gel Prepared Ni–Mo–Mg Oxide Catalyst", *Materials Letters* 60 (2), 3735–3740.

Khasim, S., Raghavendra, C., Revanasiddappa, M., Sajjan, K., Lakshmi, M. & Muhammad, F. (2011), "Synthesis, Characterization and Magnetic Properties of Polyaniline-γ-Fe_2O_3 Composites", *Bulletin Material Science* 34 (7), 1557–1561.

Khazi, M. B., Aravindan, R. & Viruthagiri, Th. (2010), "Recent Advances in the Biodegradation of Phenol": A Review, A*sian J. Exp. Biol. Science*, 1 (2), 219-234.

Kirszensztejn, K, A. Szymkowiak, P. Marciniak, A. Martyla and R. Przekop, (2003).Texture of Al_2O_3-SnO_2 binary oxides system obtained via sol–gel chemistry, Applied Catalysis A: General , 245 (1) ,159–166.

Kumar,S.M., Nillohit, M., Anup, M. & Bibhutosh, A. (2012), "Synthesis, Characterization and photocatalytic Activity of α-Fe_2O_3 Nanoparticle", *Polyhedron* 33 (1), 145–149.

Kyeong Youl Jung, Seung Bin Park and Son-Ki Ihmb,2004. Local structure and photocatalytic activity of B_2O_3–SiO_2/TiO_2 ternary mixed oxides prepared by sol–gel method Applied Catalysis B: Environmental 51 (2004) 239–245.

Liotta, L.F., Gruttadauria, M., Carlo, G. D., Perrini, G. & Librando, V. (2009),"Heterogeneous catalytic Degradation of Phenolic Substrates", *Journal of Hazardous Materials*, 162(3), 588–606.

Liou, R., Chen, Sh. H., Hung, M.Y., Hsu, Ch. Sh. & Lai, J.Y. (2005), "Fe (III) supported on resin as effective catalyst for the heterogeneous oxidation of phenol in aqueous solution", *Chemosphere* 59 (4), 117–125.

Liu, W.J., Zenga, F. X., Jianga, H., Zhang X. S. & Li, W.W. (2012), "Composite Fe_2O_3 and ZrO_2-Al_2O_3

Photocatalyst: Preparation, Characterization and Studies on the Photocatalytic Activity and Chemical Stability", *Chemical Engineering Journal* 180 (1), 9–18.

Lovestam, G., H. Rauscher, H., Roebben, G., Kluttgen, B.S., Gibson, N., Putaud, J. & Stamm, H. (2010), "Consideration on Definitions of Nanomaterial for Regulatory Purposes", EUJRC Reference Report, 40 p

Ma, R.T., Zhao, H.T. & Zhang, G. (2010), "Preparation, Characterization & Microwave Absorption Properties of Pani-$Co_{0.5}Zn_{0.5}Fe_2O_4$ Nanocomposite", *Materials Research Bulletin* 45(5), 1064–1068.

Mohammad, D., Ayati, B., Ganjidoust, H. & Sanjabi, S. (2012), "Kinetics Study of Photocatalytic Process for Treatment of Phenolic Wastewater by TiO_2 Nanopowder Immobilized on Concrete Surfaces", *Toxicological and Environmental Chemistry*, 94 (6), 1086-1098.

Mostafa Feyzi, Shirin Nadri and Mohammad Joshaghani, (2012). Catalytic Performance of Fe-Mn/SiO_2 Nanocatalysts for CO Hydrogenation, *Journal of Chemistry, Hindawi Publishing Corporation,* 2013, Article ID 973160, 10 pages. http://dx.doi.org/10.1155/2013/973160.

Reyad Awwad, Sh., (2010), Photocatalytic Degradation of Phenol using Fe-TiO_2 by Different Illumination Sources", *International Journal of Chemistry* 2 (2), 10-18.

Salaices, M., Serrano, B., de Lasa, H.I. (2004), " Photocatalytic Conversion of Phenolic Compounds in Slurry Reactors", *Chemical Engineering Science* 59(1), 3-15.

Shannon, R.D. (1976), "Revised Effective Ionic Radii and Systematic Studies of Interatomic Distances in Halides and chalcogenides", *Acta Crystallogr,* A32: 75.

Shawabkeh, R. A., Chessman, O. A. & Bisharat, G. I. (2010), "Photocatalytic Degradation of Phenol using Fe-TiO_2 by Different Illumination Sources", *International Journal of Chemistry* 2(2), 10-18.

Shukla, S.K., Bharadvaja, A., Tiwari, A., Parashar, G.K., Dubey, G.C.(2010), "Synthesis and characterization of Highly Crystalline Polyaniline Film Promising for Humid Sensor, *Advanced Mataterials Letter* 1(2), 129-134.

Sozeri, H., Kurtan, U., Topkaya, R., Baykal A. & Toprakd, M.S. (2012), "Pani–$Co_{0.5}mn_{0.5}fe_2o_4$ Nanocomposite: Synthesis, Characterization and Magnetic Properties Evaluation, *Ceramics International* 20(3), 45-60.

Tao,Y., Cheng, Z. L., Ting K. E. &Yin, X. J. (2012), "Photocatalytic Degradation of Phenol Using Nanocatalyst: Mechanism and Kinetics", *Journal of Catalysts*, 2013, Article ID 364275, 6 pages http://dx.doi.org/10.1155/2013/364275.

Ting Ke Tseng, Yi Shing Lin, Yi Ju Chen & Hsin Chu (2010), "A Review of Photocatalysts Prepared by Sol-Gel Method for VOCs Removal", *International Journal of Molecular Science* 11(4), 2336-2361.

Umar, I.G. & Abdullah, A. H. (2008), "Heterogeneous Photocatalytic Degradation of Organic Contaminants over Titanium Dioxide: A review of fundamentals, progress and problems", *Journal of Photochemistry and Photobiology C: Photochemistry Reviews,* 9(1), 1–12.

Wenzong,Y., Wenzhong W. & Songmei, S. (2010), "Photocatalytic Degradation of Phenol over cage-like Bi_2MoO_6 Hollow Spheres under Visible-Light Irradiation", *Catalysis Communications* 11(3), 647–650.

Xianliang, F., Wenming, T., Lei, J. & Shifu Chen (2012), "V_2O_5-Al_2O_3 Composite Photocatalyst: Preparation, Characterization, and the role of Al_2O_3", *Chemical Engineering Journal* 180 (1), 170–177.

Yan, L. & Sun, D. (2007), "Development of Fe_2O_3-CeO_2-TiO_2/γ-Al_2O_3 as Catalyst for catalytic Wet Air Oxidation of Methyl Orange Azo Dye under Room Condition", *Applied Catalysis B: Environmental* 72(8), 205–211.

6. Authors Biography

Mr.Tesfa Oluma Fufa was born on 12 September 1985 at Sibu Sire, Wellega, Oromia Region, Ethiopia. He received his B.Ed Degree of Chemistry from Dire Dawa University, Dire Dawa, Ethiopia, in 2009. He received his M.Sc Degree of inorganic chemistry from Haramaya University, Haramaya, Ethiopia, in 2013. Currently, he is working with academic rank of Lecturer at Haramaya University, Haramaya, Ethiopia.

Dr.Abi Tadesse Mengesha was born on 03 August 1952, at Wello, Amhara Region, Ethiopia. He received his B.Sc degree of Chemistry and M.Sc degree of Inorganic Chemistry from Addis Ababa University, Ethiopia and Ph.D degree from Pretoria University, South Africa. Currently, he is working with academic rank of Associate Professor at Haramaya University, Haramaya, Ethiopia.

Prof. O.P. Yadav was born on 10 January 1920, in India. He received his B.Sc degree of Chemistry and M.Sc degree of Physical Chemistry from India University, India and Ph.D degree also from India University, India. Currently, he is working within academic rank of Professor at Haramaya University, Haramaya, Ethiopia.

The IISTE is a pioneer in the Open-Access hosting service and academic event management. The aim of the firm is Accelerating Global Knowledge Sharing.

More information about the firm can be found on the homepage:
http://www.iiste.org

CALL FOR JOURNAL PAPERS

There are more than 30 peer-reviewed academic journals hosted under the hosting platform.

Prospective authors of journals can find the submission instruction on the following page: http://www.iiste.org/journals/ All the journals articles are available online to the readers all over the world without financial, legal, or technical barriers other than those inseparable from gaining access to the internet itself. Paper version of the journals is also available upon request of readers and authors.

MORE RESOURCES

Book publication information: http://www.iiste.org/book/

IISTE Knowledge Sharing Partners

EBSCO, Index Copernicus, Ulrich's Periodicals Directory, JournalTOCS, PKP Open Archives Harvester, Bielefeld Academic Search Engine, Elektronische Zeitschriftenbibliothek EZB, Open J-Gate, OCLC WorldCat, Universe Digtial Library , NewJour, Google Scholar